Proximity Coupled Microstrip Elements and Interconnects of Arbitrary Shape in Multilayered Media †

Ming-Ju Tsai and Nicolaos G. Alexopoulos
Electrical Engineering Department
University of California, Los Angeles
Los Angeles, CA 90024

† This research was supported by TRW-UC Microelectronics Contract DP2815219S and U.S. Army Research Grant DAAH 04-93-G-0228.

Abstract

The performance of microstrip elements of arbitrary shape as resonators, directional couplers, antennas and multilevel interconnects is examined in this paper. The mixed potential integral equation (MPIE) method is employed with triangular patch functions to model microstrip elements of arbitrary shape. The model is equally applicable to microstrip circuit and/or microstrip antenna design. The paper includes thorough investigation of the excitation mechanism. This presentation will focus on proximity coupled microstrip elements and multilevel interconnects.

I. INTRODUCTION

This paper focuses on the modeling of microstrip elements of arbitrary shape in multilayered media. Emphasis will be placed on the impact of the excitation mechanism on circuit performance. Thus, for example, in the case of resonators, the change in resonant frequency due to the presence of proximity coupling from the embedded microstrip feedline will be presented. Several classes of microstrip resonators of arbitrary shape will be considered including circular, elliptical, polygonal ring geometries and spiral elements (Archimedean and equilateral). The microstrip feedline will be printed at an interface below or above the resonator in a multilayered medium. The use of these classes of resonators for the design of filters, circulators, directional couplers and antennas will be discussed with practical examples.

The MPIE method [1]-[3] combined with the triangular patch expansion function [4] is developed to model general microstrip geometries. The MPIE was found to be better for numerical modeling than the previously used electric field integral equation (EFIE) techniques and the spectral-domain analysis [5]. Furthermore, a better physical interpretation of current flow and field distribution is obtained with this approach. The triangular basis function has been successfully used in the past to solve irregular scatterers [4, 6]. It describes the vector surface current, and matches the boundary conditions with no normal components along the boundary edges. It can also be used to represent non-planar current flow.

The MPIE method presented here starts from meshing the whole microstrip geometry with small triangular faces. The algorithm developed by McKinzie [7] is used in this analysis. Both spatial-domain Green's functions, as obtained from vector and scalar potentials respectively, are evaluated by computing a Sommerfeld-type integral. By means of the moment method (MM) a matrix equation can be set up. Several numerical techniques are applied to speed up calculation. They will be introduced in the next section. Three examples are shown and are discussed in section III.

II. THEORY

For a generalized multilayered medium shown in Fig. 1, the EFIE can be set up, by applying the boundary condition of zero tangential field on metal surface S, as

$$\hat{n} \times \vec{E}^{inc}(\vec{r}) = -\hat{n} \times \int_s \overline{\overline{G}}_E(\vec{r} \mid \vec{r}_s) \cdot \vec{J}_s(\vec{r}_s)\, dS_s \qquad (1)$$

CH3577-4/95/0000-0475$01.00 © 1995 IEEE

where $\overline{\overline{G}}_E$ is the electric field dyadic Green's function, and $\vec{J}_s$ is the surface current distribution. For simplicity, we neglect, in the present examples, the conductor and dielectric losses. If we introduce the magnetic vector potential ($\vec{A}$) and charge scalar potential (V) as $\vec{E} = -j\omega\vec{A} - \nabla V$, then Eq.(1) can be rewritten as an MPIE:

$$\hat{n} \times \vec{E}^{inc}(\vec{r}) = \hat{n} \times \quad [\quad j\omega \int_s \overline{\overline{G}}_A(\vec{r} \mid \vec{r}_s) \cdot \vec{J}_s(\vec{r}_s)\, dS_s + \nabla \int_s G_q(\vec{r} \mid \vec{r}_s) q_s(\vec{r}_s)\, dS_s] \quad (2)$$

where $\overline{\overline{G}}_A$ and G_q are the dyadic Green's function for $\vec{A}$ and V, respectively. Both $\overline{\overline{G}}_A$ and G_q are derived in the spectral domain analytically first, then can be evaluated in the spatial domain through the computation of Sommerfeld-type integrals. $\vec{J}_s$ and q_s are the unknown distribution of surface electric current and charge. They are connected to each other by the continuity equation. The reason to use MPIE instead of EFIE is that it is not necessary to use two-dimensional infinite integrals with highly oscillating functions. After removing the singular term, which occurs when source and field points coincide and has been proven to yield closed-form results [8], only surface integrals with well-behaved functions over small areas need to be calculated.

To model the arbitrarily-shaped surface current and charge distribution, the triangular patch subdomain function, shown in Fig. 2, is defined as

$$\vec{tri}_n(\vec{r}) = \begin{cases} \frac{\ell_n}{2A_n^+}(\vec{r} - \vec{r}_{n1}) = \frac{\ell_n}{2A_n^+}\vec{\rho}_n^{\,+} & : \vec{r} \in T_n^+ \\ \frac{\ell_n}{2A_n^-}(\vec{r}_{n4} - \vec{r}) = \frac{\ell_n}{2A_n^-}\vec{\rho}_n^{\,-} & : \vec{r} \in T_n^- \\ 0 & : \text{otherwise,} \end{cases} \quad (3)$$

and is adopted to expand the unknown quantities. This representation can describe the vector current flowing, and its divergence is a constant over the associated triangular face. Furthermore, it matches the boundary condition since no normal components exist except the common edge. The grid algorithm developed in [7] is used to mesh the whole circuit to small triangular faces.

The next step is to apply Galerkin's procedure and MM to reduce MPIE to matrix form. Choosing the same current cell as the testing function and by utilizing vector identities, Eq.(2) can be reformulated as a matrix equation [Z] [I] = [V], with the following matrix elements:

$$Z_{mn} = j\omega \int_{S_m} dS \int_{S_n} dS_s [\vec{tri}_m(\vec{r}) \cdot \overline{\overline{G_A}}(\vec{r} \mid \vec{r}_s) \cdot \vec{tri}_n(\vec{r}_s)] + \frac{1}{j\omega} \int_{S_m} dS \int_{S_n} dS_s [\nabla \cdot \vec{tri}_m(\vec{r})] G_q(\vec{r} \mid \vec{r}_s) [\nabla_s \cdot \vec{tri}_n(\vec{r}_s)] \quad (4)$$

In this analysis, the delta-gap source, attached at the end of input line, is used to be the excitation mechanism. Therefore, no calculation is necessary for [V].

Several numerical techniques are applied to accelerate the computation. The most time consuming step is to evaluate the Sommerfeld integral of the spatial-domain Green's function $\overline{\overline{G}}_A$ and G_q. In this analysis, numerical quadrature method with self-convergent detection is applied in the computer codes. Because of the smooth behavior of $\overline{\overline{G}}_A$ and G_q, only a few points are computed through numerical integration, then the values of $\overline{\overline{G}}_A$ and G_q in Eq.(4) are interpolated from these constructed arrays. Moreover, the non-singular part of Z_{mn} are approximated by three-point average, while four seven-point quadratures combined with analytic expressions [8] are used to evaluate the singular parts. The filling process of impedance matrix is based on faces instead of interior edges to reduce the redundant calculation of interaction from same face pairs.

III. NUMERICAL RESULTS AND DISCUSSION

A. Resonator Elements

The resonator geometry of arbitrary shape is shown in Fig. 3. In each case the excitation is provided by microstrip line embedded on an interface above or below the resonator. Results will be shown for several ring resonator geometries. Fig. 4 shows an example of a circular ring resonator with a resonant frequency at f=12 GHz. In this example ϵ=2.2 demonstrate that this resonator is actually an efficient microstrip antenna element. For the elliptical ring resonator, shown in Fig. 5, substrate is chosen as ϵ=9.8. Results for other ring geometries will be shown during the presentation.

B. Microstrip Radial Stubs

Fig. 6 shows the transmission coefficient of single-layered microstrip shunt-connected radial stub. Compared to the measurement in [9], good agreement over wide frequency range is obtained. Additional stub geometries will also be shown as a comparative study in stub design.

C. Mitered-Bend Overlap Coupler

The triangular patch function is well suited for mitered-bend microstrip discontinuity design. The coupling length has been changed to investigate the best performance for a directional coupling. Fig. 7 shows the scattering parameters of port #2 with quarter guided-wavelength coupling length. Since the whole circuit is not matched very well, the low reflection and isolated port can not be achieved. An optimized design will be shown during the presentation.

IV. CONCLUSION

The full-wave spatial-domain analysis has been used to develop a generalized dynamic model for arbitrarily-shaped microstrip circuits and antennas in multilayered structures. The results presented show excellent properties and find promising applications in MMIC coupler and filter designs. This analysis provides an accurate and flexible algorithm to model microstrip discontinuities as well as microstrip antennas.

References

[1] K. A. Michalski, "The mixed-potential electric field integral equation for objects in layered media," *Arch. Elek. Übertragung.*, vol. 39, pp. 317-322, Sep.-Oct. 1985.

[2] J. R. Mosig and F.E. Gardiol, "General integral equation formulation for microstrip antennas and scatterers," *IEE proc. H*, vol. 132, no. 7, pp. 424-432, Dec. 1985.

[3] J. R. Mosig, "Arbitrarily shaped microstrip structures and their analysis with a mixed potential integral equation," *IEEE Trans. Microwave Theory Tech.*, vol. MTT-36, no. 2, pp. 314-323, Feb. 1988.

[4] S. M. Rao, D. R. Wilton and A. W. Glisson "Electromagnetic scattering by surfaces of arbitrary shape," *IEEE Trans. Antenna Propagat.*, vol. AP-30, pp. 409-418, May 1982.

[5] M. J. Tsai, "Via hole modeling for multi-layered microstrip circuits," Master Thesis, UCLA, 1993.

[6] K. A. Michalski and D. Zheng, "Electromagnetic scattering and radiation by surfaces of arbitrary shape in layered media, part II: implementation and results for contiguous half-spaces," *IEEE Trans. Antenna Propagat.*, vol. AP-38, pp. 345-352, March 1990.

[7] W. E. McKinzie, "Electromagnetic modeling of conductor-backed aperture antennas and circuits of arbitrary shapes," Ph.D. dissertation, UCLA, 1992.

[8] D. R. Wilton, S. M. Rao, A. W. Glisson, D. H. Schaubert, O. M. Al-Bundak and C. M. Butler, "Potential integrals for uniform and linear source distribution on polygonal and polyhedral domains," *IEEE Trans. Antenna Propagat.*, vol. AP-32, no. 3, pp. 276-281, Mar. 1984.

[9] F. Giannini, M. Ruggieri and J. Vrba, "Shunt-connected microstrip radial stubs," *IEEE Trans. Microwave Theory Tech.*, vol. MTT-34, no. 3, pp. 363-366, Mar. 1986.

FIGURES

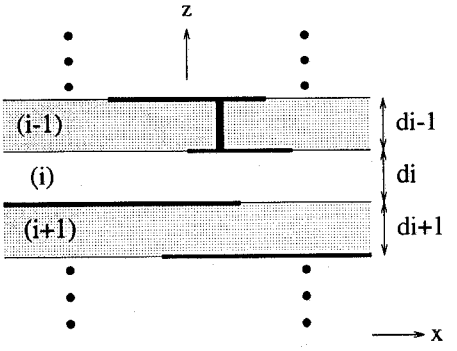

Figure 1: Generic multilayered medium.

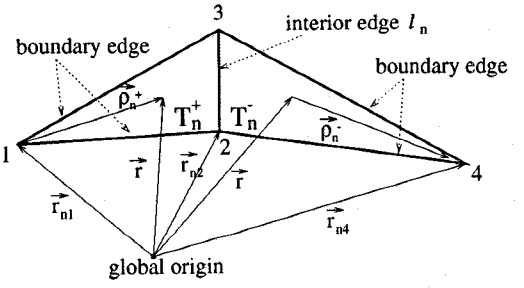

Figure 2: Triangular patch subdomain function.

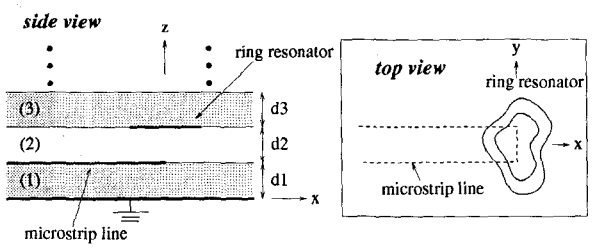

Figure 3: Ring resonator of arbitrary shape.

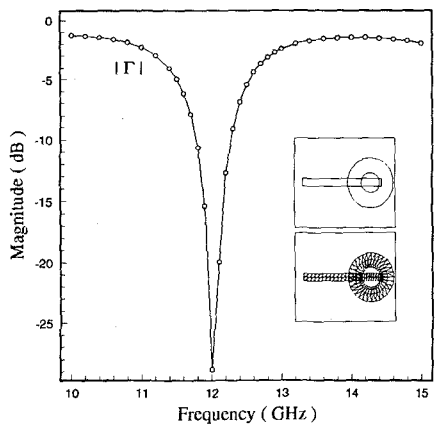

Figure 4: Reflection coefficient of microstrip circular ring resonator. ϵ_{r1}=ϵ_{r2}=2.2, d_1=d_2=0.794mm, line width=2.25mm, R_{out}=7.5mm, R_{in}=3mm, coupling length from center=3.75mm, 224 triangular faces in total.

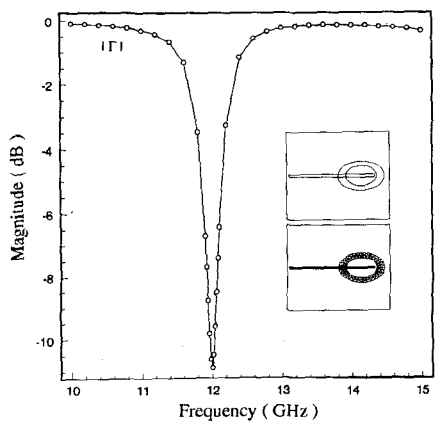

Figure 5: Reflection coefficient of microstrip elliptical ring resonator. ϵ_{r1}=ϵ_{r2}=9.8, d_1=d_2=0.635mm, line width=0.406mm, R_{out}=3.385mm, R_{in}=2.241mm, scaling factor (a,b)=(1.2, 0.748), coupling length from center=2.363mm, 296 triangular faces in total.

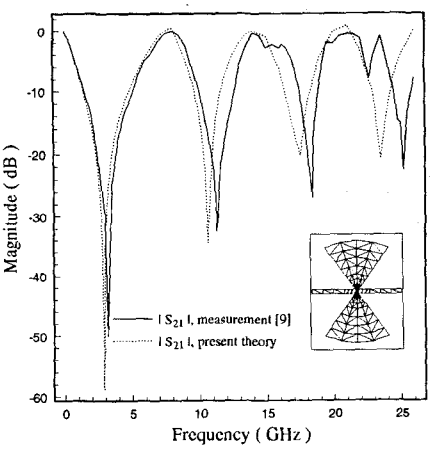

Figure 6: Transmission coefficient of microstrip radial stub. ϵ_r=10.0, substrate thickness=0.635mm, line width=0.6mm, radius=7.5mm, radial angle=60°, 212 triangular faces in total. Measurement is from [9].

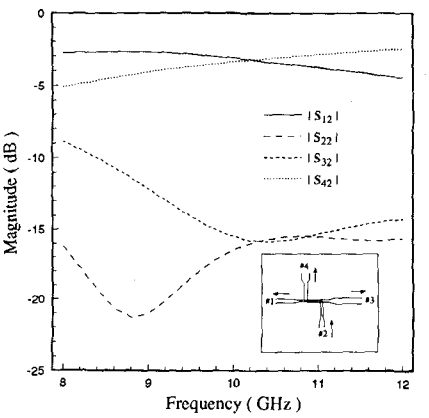

Figure 7: Scattering parameters of mitered-bend coupler. ϵ_r=10.2(top),2.2(bottom); thickness=0.635mm(top), 0.635mm(bottom);
microstrip line width=1.854mm(top),1.112mm(bottom); coupling line width=0.742mm(top),0.445mm(bottom); overlap length=3.708mm; 368 triangular faces in total.